

Composites of Poly(3,4-ethylenedioxythiophene) and CoFe_2O_4 Nanoparticles: Composition Influence on Structural, Electrical, and Magnetic Properties

Matías Lanús Mendez Elizalde, Carlos Acha, Fernando V. Molina, and P. Soledad Antonel*

Cite This: *J. Phys. Chem. C* 2020, 124, 6884–6895

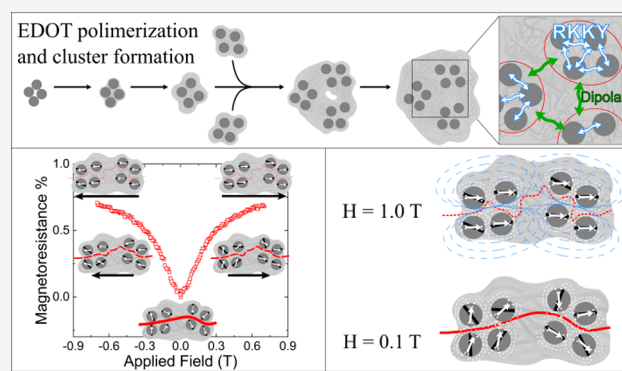
Read Online

ACCESS |

Metrics & More

Article Recommendations

ABSTRACT: Composites of magnetic CoFe_2O_4 nanoparticles (MNP) in a poly(3,4-ethylenedioxythiophene) matrix at different ratios have been synthesized. Composites were characterized by electron microscopy, X-ray diffraction, thermal analysis, electrical conductivity, magnetization, and magnetoresistance studies. In the composites the MNP appear clustered, with an interparticle distance essentially constant, but where two regimes are distinguished for cluster separation: for high MNP concentrations an intercluster separation similar to the interparticle distance is found, while for low MNP contents the distance between clusters is larger than the interparticle separation. The electrical conductivity increases with polymer content, but being always far lower than general effective medium theory expectations. This indicates that the effect of MNP effect on polymer conduction is probably related to the generation of mechanical stress both by introducing additional scattering centers and by producing different arrangement of the polymer chains, compared with the pure PEDOT. The magnetization studies reveal the existence of the RKKY interaction, which couples ferromagnetically the MNP located in a cluster, while the dipolar interaction dominates the interaction between clusters. Magnetoresistance was studied for these composites, with a maximum value close to 0.7% at 0.7 T for the lowest polymer content. The magnetoresistance correlates very well with the reversible part of the magnetization, indicating that its possible origin should be associated with polymer mechanical deformation due to the magnetic-field-induced rotation of the MNP.



INTRODUCTION

Composite materials based on conducting polymers and magnetic nanoparticles (MNP) have received much attention in the past years.^{1–11} Conducting polymers, on the one hand, have interesting chemical, conducting, mechanical, and optical properties leading to a high number of proposed applications.^{12–15} In particular, poly(3,4-ethylenedioxythiophene) (PEDOT) is highly interesting because of its excellent environmental stability,¹⁶ high electrical conductivity,¹⁷ and transparency in the doped state.¹⁸ On the other hand, MNP are also highly interesting materials due to their potential applications in different fields.^{19,20} In particular, spinel ferrite nanoparticles have been intensively investigated, and among them, cobalt ferrite (CoFe_2O_4) is especially interesting because it is a hard material from the magnetic point of view and has moderate saturation magnetization, exhibiting also excellent stability.^{21,22} Also, it has promising application for micro-electronic devices, actuators, and transducers. Thus, by combination of conducting polymers and MNP, it is possible to obtain materials with high magnetic susceptibilities and high electrical conductivities, giving rise to applications in nonlinear

optics, electromagnetic interference shielding, microwave absorption, electrochemical supercapacitors, ion adsorption, and electrocatalysis, among others.^{8,11,23–28} All these applications underline the importance of the study of these composites from an applied point of view, besides the fundamental interest. In particular, there are few reports concerning composites based on PEDOT and MNP, which studies include microwave absorption behavior,²⁸ adsorption of heavy metal ions,²⁹ and catalytic performance.²⁵ Another interesting property shown by conducting polymers, including PEDOT, is the magnetoresistance effect (OMAR),^{30–34} mainly associated with the spin correlations between different carriers, while the standard magnetoresistance (MR) refers to the phenomenon in which the electrical resistance of a material

Received: December 3, 2019

Revised: February 19, 2020

Published: March 5, 2020

changes when an external magnetic field is applied to it. This latter effect was also studied in MNP, in particular magnetite³⁵ and ferrites.^{36,37} It is proposed that materials that show MR can be applied in spintronics, electronics, computer memory, storage technology, and magnetoresistance sensors.^{34,38–40} For these reasons, there are several challenges in the design of novel and suitable magnetic materials that show an improved magnetoresistance effect. Within these materials, composites based on conducting polymers and MNP are attractive candidates for this end,^{41,42} although to the present their magnetoresistance effect has not been studied deeply. Is the MR effect related to the local magnetic field generated by the MNP? Does the metallic nature of the polymeric matrix affect the magnetic interactions and then influence the MR effect? How can the MR be maximized? To answer these questions, it is necessary to perform an exhaustive and complete physicochemical characterization in order to have tools allowing to synthesize a material with the desired properties, this is to say, to tune the physicochemical properties through the synthetic route employed.^{43,44} To the best of our knowledge, there are relatively few reports that show the dependence of the final properties of PEDOT-based composites (such as electrical conductivity, magnetic properties, and morphology) on the conducting polymer:MNP molar ratio in the composites.^{3,41,45} In a recent study,⁴⁶ the thickness of the polymer shell of core–shell magnetite–PEDOT microspheres was tuned by varying the magnetite:monomer molar ratio. Moreover, to have a better understanding of the influence of the composition on the final properties, it is important to study the magnetic interactions between the different components in the composites. To the present, and to the best of our knowledge, there are no reports concerning the type and magnitude of the magnetic interactions in composites based on PEDOT conducting polymer and CoFe₂O₄ nanoparticles. The change in the type and magnitude of the magnetic interactions with the composite composition is a fundamental study to gain insight, also, into the potential application of these materials in the magnetoresistance field.

In this work, composites based on PEDOT and MNP of CoFe₂O₄ were chemically synthesized by varying the EDOT:MNP molar ratio in the feed solution to obtain materials with different compositions. Morphology, crystallinity, electrical conductivity, magnetoresistance, and magnetic properties, focusing on the type and magnitude of the interactions, were thoroughly studied and analyzed to understand their correlations with the overall electric and magnetic properties.

MATERIALS AND METHODS

AR grade chemicals, supplied by Sigma-Aldrich, and high purity water (18 MΩ cm) from a Milli-Q system were employed throughout. Ethylenedioxythiophene (EDOT) was used as received.

Synthesis of Cobalt Ferrite Nanoparticles. The synthesis of CoFe₂O₄ nanoparticles was performed by following Antonel et al.⁴⁷ Briefly, 22.25 mL of a solution containing 0.450 M FeCl₃·6H₂O and 0.225 M CoCl₂·6H₂O (2:1 Fe(III)–Co(II) molar ratio), in 0.4 M HCl, was added dropwise to 200 mL of 1.5 M NaOH under constant and high speed mechanical stirring. The synthesis temperature was set at 80 °C by using a water-jacketed reaction vessel with a circulating thermostatic bath. Dark brown CoFe₂O₄ nanoparticles precipitated immediately after the first drops of the Fe(III)–Co(II)

solution. The temperature of synthesis and the high-speed mechanical stirring were kept constant during the addition of the cationic solution. After the addition of this solution, the reaction media was maintained at 80 °C, at high-speed stirring, for 2 h. The CoFe₂O₄ nanoparticles were separated by centrifugation at 12000g for 20 min at room temperature. The pellet was washed with Milli-Q water, repeating the cycles of washing–centrifugation until neutral pH of the supernatant was reached (about 10 times). Finally, the CoFe₂O₄ nanoparticles were dried by using a vacuum oven at 40 °C for 24 h.

Synthesis of CoFe₂O₄–PEDOT Composites and PEDOT. CoFe₂O₄–PEDOT composites were synthesized by following Ohlan et al.,⁴⁸ with some modifications. First, CoFe₂O₄ nanoparticles were added to a 0.1 M dodecylbenzenesulfonic acid (DBSA) solution (used as both protecting agent and acid media) in a CoFe₂O₄:DBSA molar ratio of 0.33. To efficiently disperse the MNP and to allow DBSA adsorption onto them, strong mechanical stirring and ultrasound treatment were applied for 30 min. This was performed by placing the recipient containing the DBSA solution and MNP in an ultrasonic bath (Testlab, model TB04), operating with a power of 160 W and a frequency of 40 kHz. After that, a brown emulsion was obtained. Then, ethylenedioxythiophene (EDOT) monomer (in molar ratios with respect to CoFe₂O₄, r_{EDOT} , of 2, 5, and 10) was added, keeping the reaction mixture in the same conditions for 1 h. Finally, ammonium persulfate (APS), in a molar ratio of 1:1 with respect to EDOT, was added, and the reaction mixture was kept 3 h always under ultrasound treatment and mechanical stirring. The product was demulsified with an equal volume of isopropyl alcohol. The blue precipitate obtained was separated by centrifugation at 15000g for 10 min at 17 °C, washed with ethanol and Milli-Q water to remove the excess of reactants and oligomers, and dried at room temperature for 24 h.

As it was mentioned above, the synthesis was performed for different values of the molar ratio in the feed:

$$r_{\text{EDOT}} = \frac{n_{\text{EDOT}}}{n_{\text{CF}}} \quad (1)$$

where n_{EDOT} and n_{CF} are the mole numbers of EDOT monomer and CoFe₂O₄, respectively.

For comparison, the PEDOT–DBSA polymer was synthesized under the same conditions as CoFe₂O₄–PEDOT composites described above, but MNP were not incorporated in the reaction media.

X-ray Diffraction (XRD) Measurements. X-ray powder diffraction analysis of nanoparticles and composites was performed with a Philips X-Pert diffractometer using Cu K α radiation ($\lambda = 0.154056$ nm); the average crystallite size was determined via the Scherrer equation

$$d_{\text{C}} = \frac{A\lambda}{\beta \cos(\theta)} \quad (2)$$

where A is a shape factor, taken here as 0.9, β is the full width at half-maximum of the peak, and θ is the corresponding Bragg angle.

Electron Microscopy Studies. The particle size and morphology of particles and composites were studied by scanning electron microscopy (SEM) and transmission electron microscopy (TEM). SEM analysis was performed using a Zeiss Supra 40 Gemini microscope equipped with an

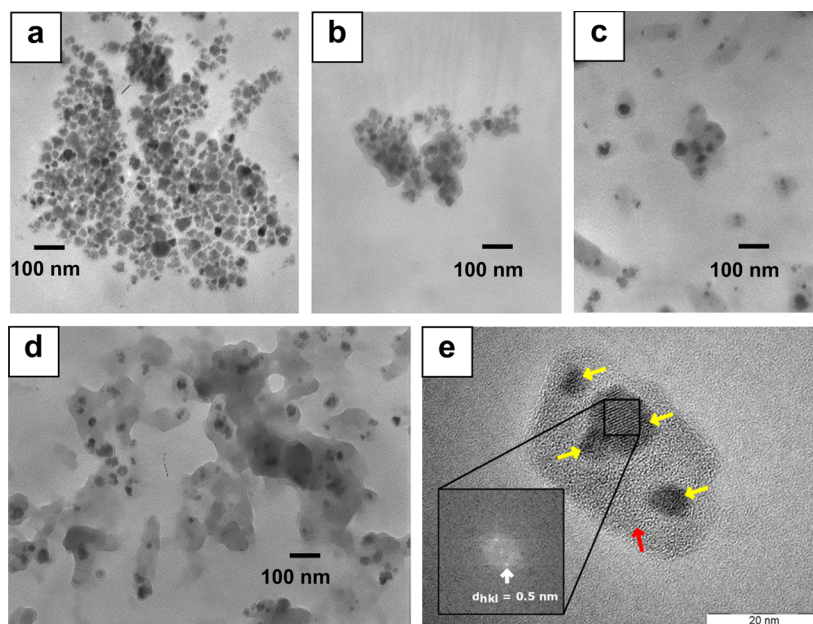


Figure 1. TEM and HR-TEM images of CoFe_2O_4 nanoparticles and CoFe_2O_4 -PEDOT composites: (a) TEM image of CoFe_2O_4 nanoparticles after polymerization treatment (without monomer); (b) TEM image of composite with $r_{\text{EDOT}} = 2$ (c) TEM image of composite with $r_{\text{EDOT}} = 5$; (d) TEM image of composite with $r_{\text{EDOT}} = 10$; (e) HR-TEM image of composite with $r_{\text{EDOT}} = 5$, yellow arrows: MNP; red arrow: PEDOT. Inset: FFT analysis of a 40 nm^2 area of a CoFe_2O_4 nanoparticle region.

EDS detector. The samples were prepared by placing a small amount of each solid (nanoparticles or composites) on one side of a carbon tape. EDS measurements were performed in the same experiment. TEM observation was performed by using a transmission electron microscope (Philips EM 301). High-resolution transmission electron microscopy (HR-TEM) bright-field imaging was performed by using a transmission electron microscope (Philips CM200 UT) with a LaB6 thermoelectric emission filament and ultra-Twin lens with a resolution of 0.19 nm. Each material (nanoparticles or composites) was suspended in acetone, and $\sim 10 \mu\text{L}$ of each suspension was dripped on a TEM grid and dried prior to insertion into the TEM column.

Thermal Analysis. Thermogravimetric analysis (TGA) of CoFe_2O_4 nanoparticles, CoFe_2O_4 -PEDOT composites, and PEDOT polymer was performed by using a simultaneous thermobalance TG-DTA 50 (Shimadzu). The TGA thermograms were recorded for 10–20 mg of each sample at a heating rate of $10 \text{ }^\circ\text{C}/\text{min}$ in the temperature range of 25–800 $^\circ\text{C}$ under an air atmosphere.

Fourier Transform Infrared Spectroscopy (FTIR) Characterization. The infrared (IR) measurements of composites, nanoparticles, and polymer were performed by using a FTIR Nicolet 8700 spectrometer in the range 400–4000 cm^{-1} , with a resolution of 4 cm^{-1} . The samples were pressed into pellets prepared by dispersing 0.5 mg of each one in 150 mg of KBr. For each sample, 32 scans were accumulated.

Electrical Conductivity Measurements. The DC conductivity of the different samples was measured on pressed circular pellets (1 cm diameter) by using a Teq-03 (Nanoteq, Buenos Aires, Argentina) potentiostat under computer control. Following Ohm's law, a known current was applied, and the potential difference was measured and averaged during 120 s. The pellet thickness was measured with a caliper to compute the conductivity.

Magnetization and Magnetoresistance Studies. A Lakeshore 7400 vibrating sample magnetometer (VSM) was used for recording magnetization curves at room temperature. The samples were prepared by packing with Teflon tape 10–20 mg of each composite. Also, two different primary remanent magnetization curves were measured at room temperature: isothermal remanent magnetization (IRM) and DC demagnetization (DCD) curves. For the IRM experiments, initially the sample was totally demagnetized at room temperature. Then, a small external field H was applied and subsequently removed, and the remanence was measured, M_{IRM} . The process was repeated increasing the external magnetic field up to 1 T. At this field, the remanence reaches its saturation value, $M_{\text{IRM}}(\infty)$. For the DCD curves, first the sample was saturated. Then, a small external field H , in the direction opposite to the magnetization, was applied. Finally, the external field was switched off, and the remanence was measured, M_{DCD} . This procedure was repeated, increasing the field H , until the saturation in the opposite direction is reached.

The resistance of the different samples was also measured in the presence of an applied magnetic field. Contacts using copper wires (100 μm of diameter), attached with silver paste to the pellets and disposed in a planar configuration, were used to perform standard two- and four-terminals techniques, with similar results in both cases. In this way, the contact resistance and the thermoelectric voltages of each terminal can be ruled out, disregarding their contribution to the measurement of the bulk resistance. To avoid overheating, measurements were performed with a Keithley 2614B source meter by applying 10 ms square voltage pulses at 1 Hz rate and by measuring the current during the 50% last part of the pulse. Details of this technique can be found elsewhere.⁴⁹ Magnetic field was varied between -0.7 and 0.7 T and incremented at a rate of 5.0 mT s^{-1} . To minimize slow drifts possibly caused by polymer degradation, as suggested by Lupton et al.,⁵⁰ the external magnetic field was applied after the electric signal was

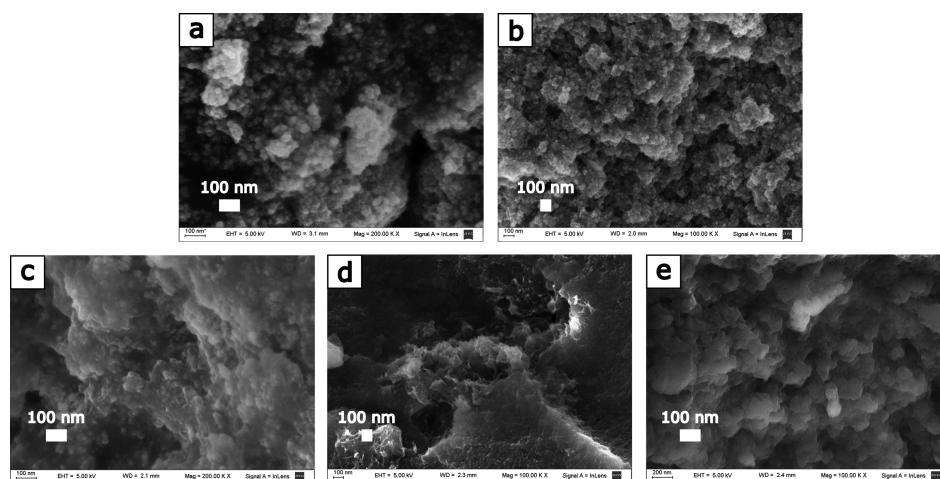


Figure 2. SEM images of CoFe₂O₄-PEDOT composites: (a) CoFe₂O₄ nanoparticles after polymerization treatment (without monomer); (b) $r_{\text{EDOT}} = 2$; (c) $r_{\text{EDOT}} = 5$; (d) $r_{\text{EDOT}} = 10$; (e) PEDOT.

stabilized. Also, multiple magnetoresistance measurements were performed and averaged.

The percent magnetoresistance (MR%) was calculated following

$$\text{MR}\% = \frac{R_H - R_0}{R_0} \times 100 \quad (3)$$

where R_H is the resistance at the applied magnetic field, H , and R_0 is the resistance in the absence of a magnetic field.

RESULTS AND DISCUSSION

Particle Size and Composites Morphology. The morphology of the cobalt ferrite particles obtained here corresponds to a spherical-like shape aggregated in clusters, very similar to those of Antonel et al.³ and Muñoz Resta et al.,⁴⁵ as they were prepared with the very same technique. In Figures 1a–d TEM images of CoFe₂O₄-PEDOT composites are shown. The TEM image of pure CoFe₂O₄ nanoparticles, after the same treatment employed for the polymerization of EDOT, is observed in Figure 1a. The particle size, as verified by TEM imaging with the aid of the ImageJ software, was found to be $d_p = 14 \pm 3$ nm, very similar to the size of CoFe₂O₄ nanoparticles without treatment. This result indicates that DBSA effectively protects CoFe₂O₄ nanoparticles from the reaction medium. Besides, the particle size is within the range of monodomain magnetic particles, which for cobalt ferrite falls between a minimum of 7–9 nm^{22,51} and a maximum of about 60–70 nm.^{52,53}

Also, in Figure 1 it is clear that high r_{EDOT} favors the dispersion of the nanoparticles as they appear more separated with the increase in r_{EDOT} . It is worth mentioning that these MNP act as catalyst for EDOT polymerization, since the polymerization yield increases significantly when they are present in the reaction medium. From Figures 1b to 1d there is a marked change in the composite morphology. For $r_{\text{EDOT}} = 2$ (Figure 1b) the polymer appears mostly covering the MNP, whereas for $r_{\text{EDOT}} = 10$ the MNP appear dispersed in a large polymer matrix, the material with $r_{\text{EDOT}} = 5$ showing an intermediate morphology. This is interpreted considering that, first, PEDOT is produced preferably around CoFe₂O₄ nanoparticles, and for higher r_{EDOT} the conducting polymer grows further giving rise to a homogeneous polymeric matrix with the nanoparticles aggregated in clusters; these in turn

dispersed in an approximately uniform way. These features were also observed previously for CoFe₂O₄-PANI³ and CoFe₂O₄-PPy⁴⁵ composites. Figure 1e shows a typical HR-TEM image of a composite with $r_{\text{EDOT}} = 5$. The nanoparticles (dark gray, indicated by yellow arrows) are surrounded by the polymer matrix (gray region, indicated by the red arrow). The high resolution of this image evidences the crystallinity of the nanoparticles in contrast with the amorphous nature of the polymer. Fast Fourier transform (FFT) analysis of the nanoparticle (Figure 1e, inset) shows a d_{hkl} of 0.5 nm, corresponding to the (111) spinel family of lattice planes. The morphology of some of the obtained materials, as observed by SEM, is shown in Figures 2a–e; Figure 2e shows an image of PEDOT without MNP for comparison.

Similarly to TEM observation, different morphologies are found for low and high values of r_{EDOT} . The composite with very low polymer content ($r_{\text{EDOT}} = 2$, Figure 2b) shows a morphology that is very similar to that of bare CoFe₂O₄ nanoparticles (Figure 2a). When increasing the PEDOT content ($r_{\text{EDOT}} = 5$, Figure 2c), composites have a relatively smooth topography, as a consequence of being dominated by the polymer presence. Finally, for high polymer content ($r_{\text{EDOT}} = 10$) the materials show a more regular surface, very similar to the pure polymer (Figure 2e). The chemical composition of the MNP was verified from SEM-EDS measurements (not shown), resulting in a Fe:Co molar ratio of 2:1, thus confirming that the product obtained was effectively CoFe₂O₄.

As was shown in Figure 1, the MNP appear aggregated in clusters in the composites with PEDOT. To have an estimation of the particle–particle separation inside each cluster, the distances between MNP were measured with the aid of the ImageJ software, and the resulting histograms are presented in Figures 3a–c, with the corresponding log-normal distributions. For each composite, ~100 particle–particle separations inside each cluster were measured. In the case of the composite with $r_{\text{EDOT}} = 10$, TEM images show that the distance between clusters is significantly larger than the particle–particle separation inside each cluster while is not the case for $r_{\text{EDOT}} \leq 5$. Therefore, in this case, about 75 distances between clusters were measured, and the resulting histograms are shown in Figure 3d, also with the corresponding log-normal distribution.

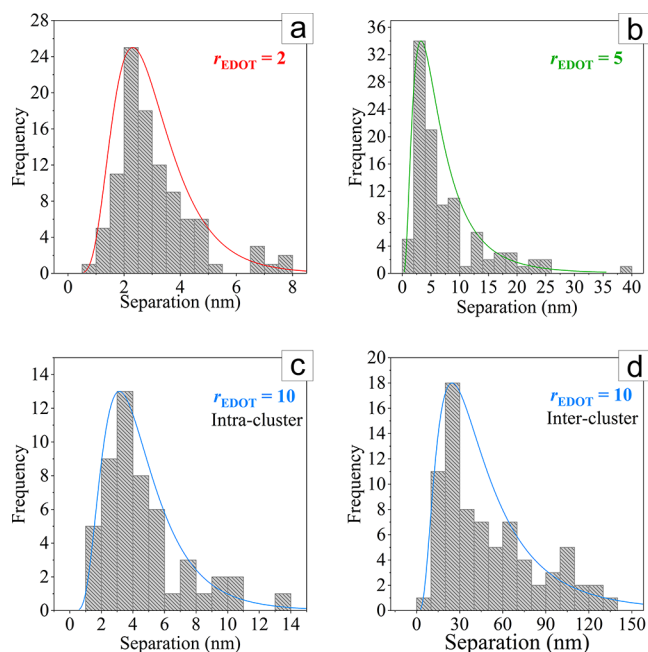


Figure 3. Particle–particle separation for CoFe_2O_4 –PEDOT composites with (a) $r_{\text{EDOT}} = 2$, (b) $r_{\text{EDOT}} = 5$, (c) $r_{\text{EDOT}} = 10$ (intracluster), and (d) $r_{\text{EDOT}} = 10$ (intercluster).

From the log-normal distributions for the particle–particle separation inside clusters in the composites with different r_{EDOT} , first the mean values and the standard deviations were calculated. The obtained values are 3 nm (standard deviation = 2 nm) for the composite with $r_{\text{EDOT}} = 2$, 7 nm (standard deviation = 4 nm) for the composite with $r_{\text{EDOT}} = 5$, and 5 nm (standard deviation = 3 nm) for the composite with $r_{\text{EDOT}} = 10$. Also, the modes were calculated, obtaining a value of 3 nm for the composite with $r_{\text{EDOT}} = 2$, 6 nm for the composite with $r_{\text{EDOT}} = 5$, and 4 nm for the composite with $r_{\text{EDOT}} = 10$. These results suggest that within experimental error the distance between MNP inside clusters remains approximately constant and is independent of r_{EDOT} . On the other hand, the cluster–cluster separation increases noticeably in the composite with $r_{\text{EDOT}} = 10$, having a mean value of 50 nm (standard deviation = 30 nm) and a mode value of 40 nm. These results indicate that in the composites the MNP are aggregated in clusters, with an interparticle separation distance essentially constant (~ 3 – 6 nm) but where two regimes can be distinguished for the intercluster separation: for high MNP concentration ($r_{\text{EDOT}} = 2$) a particle dominated composite is obtained, with an intercluster separation similar to the interparticle distance, while for a low MNP content ($r_{\text{EDOT}} = 10$), a polymer-dominated material is obtained, where the distance between clusters is clearly larger than the interparticle distance. That means that for low r_{EDOT} ($r_{\text{EDOT}} \leq 5$) the polymer appears mostly covering the MNP giving as a result an interparticle separation approximately constant. In other words, the distances between MNP are all very similar in composites with $r_{\text{EDOT}} \leq 5$ and are determined by the PEDOT layer that grows covering the MNP. On the other hand, for $r_{\text{EDOT}} = 10$ there is a higher monomer concentration in the synthesis medium, resulting in faster growth of PEDOT. Initially, the polymer appears covering the ferrite particles, resulting in clusters as before, and after that the excess monomer present

polymerizes around the clusters, resulting in larger separation between them.

Crystalline Structure. The XRD patterns of the nanoparticles obtained are shown in Figure 4, where a typical

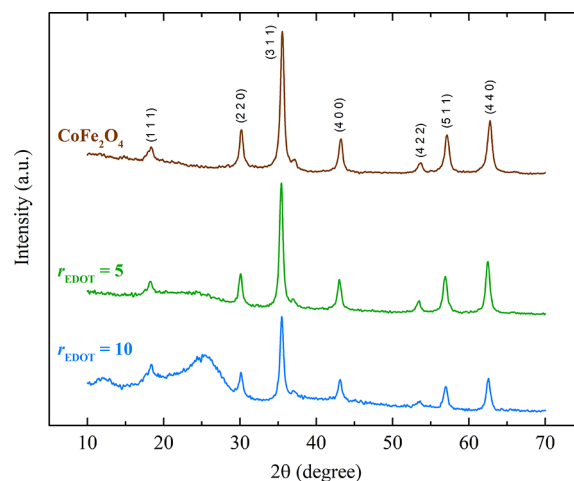


Figure 4. XRD diagram/patterns of CoFe_2O_4 nanoparticles and composites for different r_{EDOT} ratios. Nanoparticles synthesized at 80°C reveal an inverse spinel structure.

inverse spinel pattern is observed (ICDD 03-0864, JCPDS 22-1086) with the space group $Fd\bar{3}m$, very similar to that of Fe_3O_4 .^{22,54} The ferrite lattice parameter was determined by using the (311) peak and was found to be $a = b = c = 8.369 \text{ \AA}$, which is close to the values reported for CoFe_2O_4 nanoparticles.^{55–57} Besides, the obtained value of 8.369 \AA is smaller than 8.395 \AA , which corresponds to the lattice parameter of bulk CoFe_2O_4 .²² This indicates that in CoFe_2O_4 nanoparticles there are more defect sites in comparison with bulk CoFe_2O_4 —a fact that could be explained taking into account the high area/volume ratio in nanostructured systems. The diameter of the crystallites, d_c , prepared here was estimated through eq 2 by using the (311) peak, resulting in $d_c = 15.4 \text{ nm}$, which is in agreement with the TEM measurements and with the previously reported results.^{22,47}

Figure 4 also shows the XRD patterns for composites with $r_{\text{EDOT}} = 5$ and $r_{\text{EDOT}} = 10$. For smaller r_{EDOT} , the diffractograms do not show the presence of the amorphous phase associated with the polymer and are essentially identical to the one shown for pure CoFe_2O_4 nanoparticles. It is clearly observed that for a polymer dominated material ($r_{\text{EDOT}} = 10$) a broad diffraction band around $2\theta = 25^\circ$, characteristic of the low crystallinity of the polymer, is observed. Also, these results are consistent with TEM and SEM observations, which show particle-dominated composites for $r_{\text{EDOT}} = 2$ and polymer-dominated materials for $r_{\text{EDOT}} = 10$. Note that for $r_{\text{EDOT}} = 5$ the polymer band is present but very weak, consistent with a transition between NMP and polymer-dominated materials. Comparing these results with those obtained for composites of CoFe_2O_4 nanoparticles and PANI³ or PPy,⁴⁵ with PANI or PPy a higher amount of polymer is incorporated in the materials, giving as a result polymer-dominated composites even with small values for the respective monomer:ferrite molar ratios, r_{ANI} or r_{PPy} (5 in the case of PANI³ and 3.5 in the case of PPy⁴⁵). This result is consistent with the lower polymerization rate for EDOT compared with pyrrole and aniline.

Thermal Decomposition and Composite Composition. To study the thermal decomposition of the resulting composites and to gain insight into their composition, thermogravimetric analysis (TGA) in air was conducted (Figure 5); it is observed that PEDOT-DBSA is completely

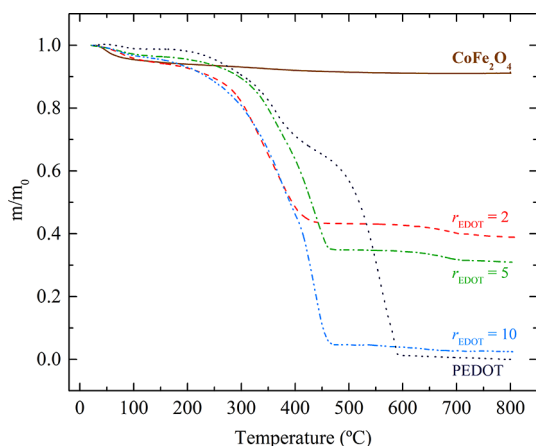


Figure 5. TGA measurements of cobalt ferrite, PEDOT, and composites, plotted as relative mass (m/m_0) as a function of temperature.

decomposed by oxidation and the ferrite particles undergo only a small mass loss, whereas the composites give intermediate results, thus confirming the composite formation. The features in Figure 5 can be explained as follows: first, when increasing the temperature T , an initial mass loss is observed, attributable to removal of water from the material; this loss ends at about 250 °C, where the curves are almost leveled. At higher temperatures, a pronounced decrease is observed, corresponding to polymer decomposition, starting at 307 ± 5 °C (as estimated from the curve derivative, not shown), with a second step at about 500 °C, and ending at ~ 600 °C for PEDOT-DBSA. This is in agreement with literature reports, where PEDOT decomposition occurs mainly in the range ~ 300 – 450 °C,⁵⁸ but mass loss is observed up to ~ 600 °C.

On the other hand, for CoFe_2O_4 -PEDOT composites the polymer decomposition starts at 260 ± 10 °C (independent of composition within experimental error) and takes place up to ~ 450 – 480 °C, without a discernible second stage. The differences comparing with the PEDOT-DBSA case can be attributed to a catalytic effect of the ferrite particles on the polymer decomposition.

Pure ferrite particles show, after some water elimination, a small decrease probably due to loss of surface hydroxyl groups. From the TGA results, the composite's composition can be estimated, assuming that the mass loss at $T < 250$ °C is due to water elimination, that the remaining mass at $T = 800$ °C corresponds to the ferrite particles with no polymer remaining, and introducing a correction for the mass change of the cobalt ferrite particles between 25 and 800 °C. The results for the CoFe_2O_4 mass fraction in the composite, f_{CF} , and the measured polymer/ferrite molar ratio, r_m , are presented in Table 1.

Electrical Conductivity. The electrical conductivity of the composites depends of the monomer–ferrite ratio, being in the range 10^{-5} – 10^{-3} S cm^{-1} with a monotonous decrease as the ferrite contents increases, as can be observed in Table 2. On the other hand, PEDOT prepared in the same conditions as

Table 1. Composite's Composition as Found by Thermogravimetric Analysis

feed composition, r_{EDOT}	measured composition, r_m	cobalt ferrite mass fraction, f_{CF}
2.0	2.1 ± 0.1	0.45 ± 0.02
5.0	3.2 ± 0.3	0.34 ± 0.03
10.0	57 ± 9	0.13 ± 0.02

Table 2. Room Pressure and Temperature Conductivities of PEDOT and Composites with Different r_{EDOT} Ratios

sample	conductivity (S cm^{-1})
composite feed composition, r_{EDOT}	
2.0	$(2.2 \pm 0.8) \times 10^{-5}$
5.0	$(4.5 \pm 1.5) \times 10^{-4}$
10.0	$(6.0 \pm 3.0) \times 10^{-3}$
PEDOT (w/o MNP)	0.3 ± 0.1

the nanocomposites gives a conductivity of 0.3 S cm^{-1} . This value is similar to several results reported for PEDOT obtained by using APS or Fe(III) as oxidizing agents. For example, Choi et al.⁵⁸ found bulk conductivities for PEDOT also synthesized with APS as oxidant and DBSA of 1 – 10 S cm^{-1} ; Morvant et al.⁵⁹ prepared thick films of PEDOT, obtaining in situ conductivities in the range 0.2 – 13.0 S cm^{-1} , depending on growth conditions; Corradi et al.⁶⁰ synthesized PEDOT at different reaction temperatures, using Fe(III) as oxidizing agent, and in this case the maximum electrical conductivity achieved was ~ 5 S cm^{-1} .

The electrical conductivity values for the composites show that the presence of the MNP highly affects the polymer electrical conductivity, since even those with the highest r_{EDOT} gives composites with low conductivities. Nevertheless, the minimum electrical conductivity value achieved ($\sim 10^{-5}$ S cm^{-1}) suggests that down to the lower r_{EDOT} explored PEDOT retains an electrical conductivity path, indicating that the polymer can percolate through the material.

Additionally, it should be mentioned that the conductivity of the composites is far away from the values expected from the general effective media (GEM) theory, which quantitatively describes the conductivity of a binary mixture as a function of the conductivities and the volume fraction of each component.^{61,62} The observed behavior indicates the strong effect that the MNP have on the conductivity of PEDOT as even a small fraction ($r_{\text{EDOT}} = 10$) decreases the conductivity of the composite far below from the expected values determined by the GEM model ($\approx 1/50$). The same effect, with similar values, was observed for PANI and Fe_3O_4 or CoFe_2O_4 composites.^{1,3} This indicates that the inclusion of MNP has a long-range effect which is probably related to the generation of mechanical stress and to a change in the electrical mobility of carriers, by both introducing additional scattering centers and by producing different arrangement of the polymer chains, compared with the pure PEDOT. This last fact is due to the initial growth of the polymer around the MNP, as suggested by SEM images, resulting in less crystallinity and thus a lower electrical conductivity.

IR Spectroscopy. Figure 6 shows the IR spectra of PEDOT, CoFe_2O_4 nanoparticles, and PEDOT- CoFe_2O_4 composites with different r_{EDOT} ratios. The IR response of PEDOT (Figure 6, top) has been reported by several authors.^{48,58,63,64} The most relevant bands of the spectra shown in Figure 6 will be discussed in the following. The

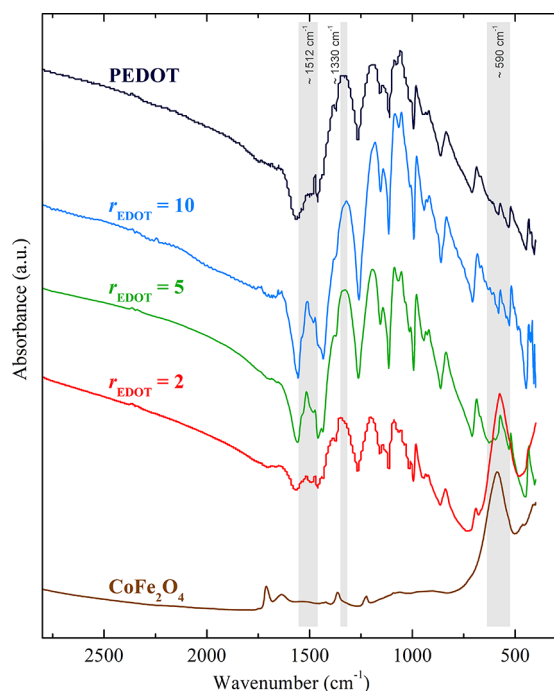


Figure 6. IR spectra of PEDOT, CoFe_2O_4 nanoparticles, and PEDOT- CoFe_2O_4 composites with different r_{EDOT} ratios.

vibrational band at around 1512 cm^{-1} corresponds to C=C or C-C ring stretching of the thiophene ring, and the one around 1330 cm^{-1} corresponds to C=C or C-C ring stretching of the quinoid structure of the thiophene ring. Vibrational bands at 1190 , 1142 , and 1055 cm^{-1} are due to C-O-C bond stretching in the ethylenedioxy group. The band around 920 cm^{-1} is originated from the ethylenedioxy ring deformation. Vibration modes of the C-S bond in the thiophene ring are also seen at 980 , 835 , and 685 cm^{-1} . In the spectrum of cobalt ferrite (bottom), on the other hand, besides surface OH vibrations ca. 3500 cm^{-1} (not shown) and other minor bands, the main lattice band at 590 cm^{-1} is clearly visible. In the composite spectra, this band shows decreasing intensity as r_{EDOT} increases, as expected. The absence of additional peaks in the range between 1600 and 1800 cm^{-1} , which would indicate carbonyl groups formation by oxidation, demonstrates that the overoxidation of the polymer can be excluded. There are some differences between the polymer bands in pure PEDOT spectrum and those in the composites, which indicates that some interaction of ferrite nanoparticles with polymer chains takes place. The most prominent change is observed in the vibrational band at 1512 cm^{-1} , which corresponds to C=C or C-C ring stretching of the thiophene ring: first, a displacement to 1520 cm^{-1} is observed for the composite with $r_{\text{EDOT}} = 2$; also, this band undergoes a splitting, giving a second one at 1470 cm^{-1} , with the A_{1470}/A_{1510} ratio (absorbance ratio) increasing with ferrite content.

Magnetization Behavior and Magnetic Interactions.

Figure 7 shows the mass magnetization, M , as a function of the applied magnetic field H for the bare particles and composites, all measured at room temperature. The curve for the bare particles is similar to others reported in the literature,^{22,45,47,51} showing hysteresis, which reveals ferromagnetic behavior. CoFe_2O_4 MNP synthesized and used in this work can be considered as magnetic monodomain particles, since their average size was found to be $d_p = 14 \pm 3\text{ nm}$, as it was

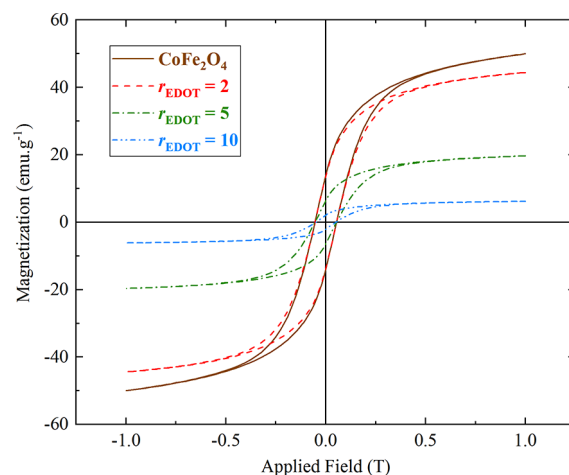


Figure 7. Magnetization curves of CoFe_2O_4 particles and composites with different r_{EDOT} measured at room temperature.

observed in TEM images. This average size lies between the critical single domain size (70 nm)^{52,53} and the superparamagnetic threshold ($7\text{--}9\text{ nm}$)^{22,51} in the case of CoFe_2O_4 MNP. That means that CoFe_2O_4 MNP having an average size between $7\text{--}9$ and 70 nm are expected to be in the monodomain regime, showing a ferromagnetic behavior at room temperature, as it was observed in the magnetization hysteresis loops shown in **Figure 7**. The fact that CoFe_2O_4 MNP show ferromagnetism at room temperature is due to their high magnetocrystalline anisotropy.^{22,65,66} Following Muñoz Resta et al.,⁴⁵ for small and single domain ferromagnetic particles, the coercivity is limited by the net anisotropy of these particles, which includes the magnetocrystalline anisotropy. Moreover, the coercivity is proportional to the anisotropy constant,⁶⁶ giving as a result that CoFe_2O_4 MNP show ferromagnetic behavior at room temperature, a result also found by other authors.^{3,22,45,47,55,65,67}

The magnetization is referred to the total composite mass, thus the curves have smaller M values as the contents of magnetic particles decreases. In particular, the maximum magnetization reached at $H = 1\text{ T}$, M_{max} (which has not yet reached its saturation value M_s), decreases as the polymer content increases because PEDOT is essentially a nonmagnetic material. M_s can be estimated by fitting the M vs H curve with a simplify law of approach to the saturation:⁶⁸

$$M = M_s \left(1 - \frac{a}{H} - \frac{b}{H^2} \right) \quad (4)$$

where a and b are appropriate constants.

The obtained M_s value for the bare CoFe_2O_4 MNP (59 emu g^{-1}) is in accordance with the values published for MNP of similar diameters.^{22,45,69}

Interestingly, although the mass fraction of the MNP for the $r_{\text{EDOT}} = 2$ composite is close to 45% of the composite mass, its M_{max} value is almost 85% of the M_{max} value for the bare particles. Also, for the $r_{\text{EDOT}} = 5$ and $r_{\text{EDOT}} = 10$ composites their M_{max} is higher than the one expected for their mass fraction of MNP. The same conclusions are found if we consider the estimated M_s values. This result is clearly indicating that the magnetization of the composites is not obeying a simple mass dilution of the MNP content. Instead, an additional ferromagnetic (FM) interaction should be playing an important role. As the MNP are embedded in

PEDOT, which is an electrical conducting material, it is possible to have a Ruderman–Kittel–Kasuya–Yosida (RKKY) mechanism which produces an indirect exchange coupling between the magnetic moment of the MNP through the electrical carriers (holes) of PEDOT.⁷⁰

The RKKY coupling will be intensely ferromagnetic for MNP that are closer than a distance d_{FM} while for longer distances (d), it will oscillate periodically from antiferromagnetic to ferromagnetic and decays as d^3 . d_{FM} can be roughly estimated as

$$d_{\text{FM}} = \frac{4.49}{2k_{\text{F}}} = \frac{4.49}{2(3\pi^2n)^{1/3}} \quad (5)$$

where k_{F} is the Fermi wave vector and n the density of free carriers. An estimation of the n value for our composites can be done as follows: As the electrical conductivity is $\sigma = n\mu q$ (where n is the density of carriers, μ their mobility, and q the elementary charge), and by considering the span of μ values reported for PEDOT materials^{71–73} synthesized with close counterions, but discarding those extremely high values, corresponding to samples prepared in a particular way to reach the most higher values of electrical conductivities ($\sigma > 6000 \text{ S cm}^{-1}$), we obtain that

$$0.1 \text{ cm}^2 \text{ V}^{-1} \text{ s}^{-1} \leq \mu \leq 10 \text{ cm}^2 \text{ V}^{-1} \text{ s}^{-1}$$

which, for our measured σ in the case of PEDOT:DBSA (0.3 S cm^{-1}), limits the n values to $2 \times 10^{23} \text{ m}^{-3} \leq n \leq 2 \times 10^{25} \text{ m}^{-3}$. In this way, we obtain from eq 5 that $3 \text{ nm} \leq d_{\text{FM}} \leq 13 \text{ nm}$. Within this interval of possible d_{FM} values, this result is in accordance with the observed behavior of M_{max} and M_{s} for the $r_{\text{EDOT}} = 2$ and $r_{\text{EDOT}} = 5$ composites. That is by considering the distance distribution of MNP for each composite (see Figure 3), it can be observed that even for the extreme case of $d_{\text{FM}} \approx 3 \text{ nm}$ a large portion of them will be coupled FM, yielding to a cluster-like magnetic behavior and, concomitantly, to an increase of their M_{max} (or equivalently of M_{s}). The RKKY influence on the M_{s} of a magnetic material surrounded by an electrical conducting matrix has been already observed, for example, in CoFe_2O_4 MNP interconnected by an Au matrix, where M_{s} presents an oscillatory damped behavior as a function of the Au width between MNP.⁷⁴

To compare more closely the above curves, they are presented in Figure 8 in the form of relative magnetization, M/M_{max} , as a function of the magnetic field. The inset shows the curves in the full range, where it is observed that all the curves merge for high field values. The main graph shows an enlarged view of the low field region, revealing that the remanence ratio, $M_{\text{r}}/M_{\text{max}}$, increases as the polymer contents increases, and also a relatively small decrease (in terms of the H range) in the coercivity H_{c} is found for the composite with $r_{\text{EDOT}} = 10$. These results suggest that in terms of coercivity the magnetic properties of the composites also show an abrupt change when passing from particle-dominated composites ($r_{\text{EDOT}} = 2$) to a polymer-dominated material ($r_{\text{EDOT}} = 10$), as it was observed in SEM and TEM observations and in XRD studies. These results, summarized in Table 3, also support the framework of a RKKY interaction between MNP and mediated by the electrons of PEDOT, already discussed for the M_{max} behavior, indicating that there is a change in the magnetic properties when the particles are included in the composite. Otherwise, if a simple “dilution” effect was taking place, all the normalized curves should be coincident. Therefore, the remanence ratio

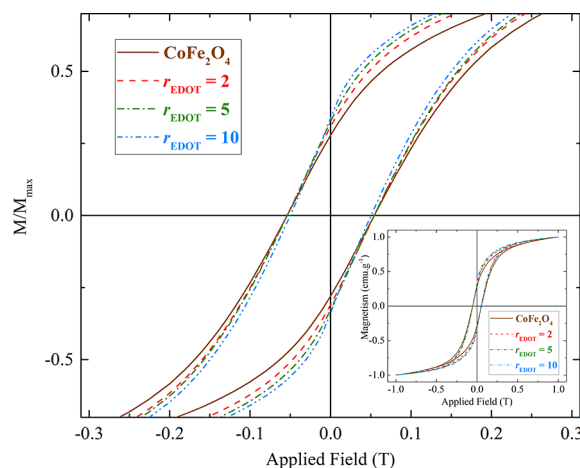


Figure 8. Normalized magnetization curves for CoFe_2O_4 -PEDOT composites, for different r_{EDOT} . The insets show the full curves, while the main graph present the curves with an enlargement around $H = 0$.

increases with r_{EDOT} , sustaining the presence of FM interactions between the magnetic NP at the expense of the polymer matrix.

To gain insight into the type and strength of interaction between MNP, isothermal remanence magnetization (IRM) and DC demagnetization (DCD) curves, both at room temperature, were measured. The results, well-known as Henkel plots,⁷⁵ are shown in Figure 9. The dashed line corresponds to eq 6 and represents the expected behavior for a noninteracting system, as predicted by the Stoner–Wohlfarth model:⁷⁶

$$\frac{M_{\text{DCD}}}{M_{\text{R}}(\infty)} = 1 - \frac{2M_{\text{IRM}}}{M_{\text{R}}(\infty)} \quad (6)$$

As can be observed, all the composites show a negative deviation from the dashed line that increases with decreasing r_{EDOT} (or the polymer content), indicating that the main interparticle magnetic interaction is dipolar.⁷⁷ This is an interesting result due to the fact that regardless of the existence of a FM coupling between MNP mediated by the RKKY interaction, the dipolar interaction is the dominant one in the magnetization and demagnetization processes.

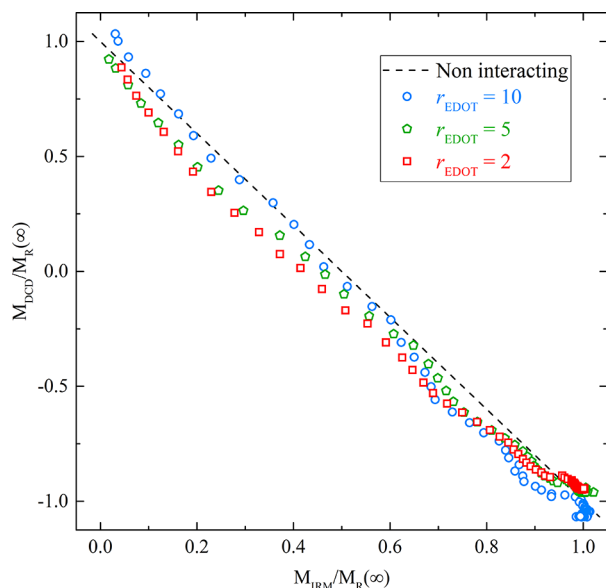
A possible interpretation of this result can be done considering that the RKKY interaction strongly couples ferromagnetically all the MNP that are at distances less than the estimated interval for d_{FM} (3–13 nm), causing them to act as a single magnetic cluster. In this framework, the IRM and DCD curves would reveal the existence of magnetic dipolar interactions between clusters. In fact, it can be observed that dipolar interactions are weak for the composite with $r_{\text{EDOT}} = 10$ and strong for the composite with $r_{\text{EDOT}} = 2$ and have an intermediate magnitude for the composite with $r_{\text{EDOT}} = 5$. This result is in accordance with the expected spatial dependence of the dipolar interaction on the average distance between magnetic interacting particles, which could then be associated with the mentioned clusters of MNP (see Figure 3).

From the IRM measurements additional information about the reversible contribution to the magnetization, M_{rev} , can be obtained, by considering the following relation:

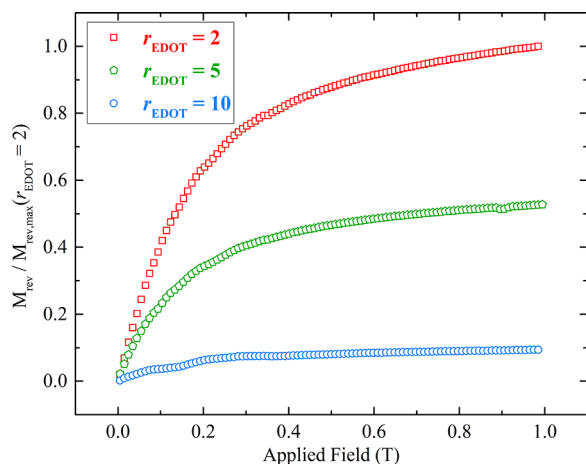
$$M_{\text{rev}}(H) = M'(H) - M_{\text{IRM}}(H) \quad (7)$$

Table 3. Coercive Field and Remanence Ratio of Cobalt Ferrite and Composites

material	CoFe ₂ O ₄	$r_{\text{EDOT}} = 2$	$r_{\text{EDOT}} = 5$	$r_{\text{EDOT}} = 10$
$H_c/10^{-4}$ T	543 ± 6	543 ± 4	541 ± 7	504 ± 7
M_r/M_{max}	0.278 ± 0.003	0.308 ± 0.002	0.326 ± 0.003	0.339 ± 0.003
M_r/M_s	0.233 ± 0.001	0.273 ± 0.002	0.289 ± 0.002	0.304 ± 0.001

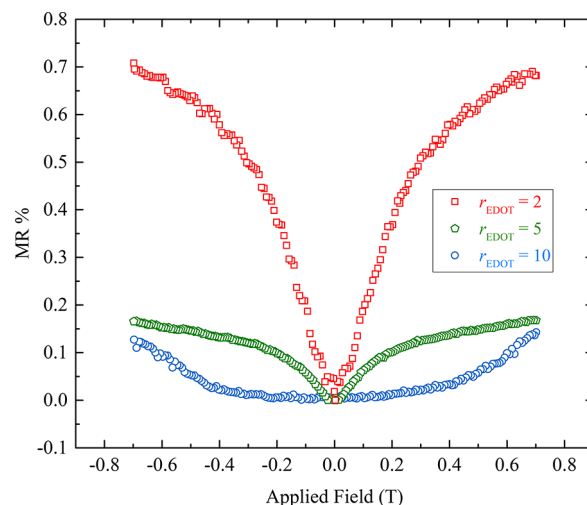
Figure 9. Henkel plot for CoFe₂O₄-PEDOT composites with different r_{EDOT} ratios.

where M' is the magnetization of the first magnetization curve and M_{IRM} as the remanent contribution, corresponds to the irreversible part of the magnetization. Results for the normalized M_{rev} are shown in Figure 10. It can be seen that

Figure 10. Normalized reversible magnetization for CoFe₂O₄-PEDOT composites with different r_{EDOT} ratios.

M_{rev} increases with the applied magnetic field for all the composites, being this increment more pronounced up to ~0.4 T. Also the increment in M_{rev} with H depends on r_{EDOT} , showing a higher value as the mass fraction of the MNP increases.

Magnetoresistance. Figure 11 shows MR%, computed from eq 3, of CoFe₂O₄-PEDOT composites at room temperature. MR% depends on r_{EDOT} , being positive and

Figure 11. Magnetoresistance for CoFe₂O₄-PEDOT composites with different r_{EDOT} ratios.

reversible and increasing in value with the applied magnetic field, as already seen by Gu et al. for composites of PANI-magnetite,⁴² by Muñoz Resta et al. for composites of PPy-CoFe₂O₄⁴⁵ and Klemm et al.⁵⁰ for PEDOT:PSS polymer. Furthermore, the magnetoresistance decreases with increasing r_{EDOT} and becomes negligible for pure PEDOT, indicating its correlation with the presence of MNP. MR% reached values up to 0.7% for composites with $r_{\text{EDOT}} = 2$ while for composites with $r_{\text{EDOT}} \geq 2$ the maximum MR% is about 0.15%. Moreover, for the composite with $r_{\text{EDOT}} = 2$ there is a linear relationship between MR% and H , in the low field region (up to ~0.3 T), which favors considering this material as a promising candidate to be applied as a magnetic sensor. To the best of our knowledge, this is the first time that magnetoresistance measurements of PEDOT-CoFe₂O₄ composites are investigated. The reversible behavior of MR% with the magnetic field and its dependence with the MNP content leads us to consider that its microscopic origin may be related to what generates the reversible part of the magnetization. Indeed, it should be noted that the shape of MR% vs H and M_{rev} vs H (Figures 11 and 10, respectively) is quite similar (at least for the composites with $r_{\text{EDOT}} = 2$ and $r_{\text{EDOT}} = 5$), effectively suggesting that the origin of the observed phenomena is the same in both cases. To better visualize the correlation between the magnetoresistance and the reversible magnetization, the relative magnetoresistance, $\text{MR}/\text{MR}_{\text{max}}$ vs the relative reversible magnetization, $M_{\text{rev}}/M_{\text{rev,max}}$ is presented in Figure 12.

Figure 12 shows that for MNP dominated materials ($r_{\text{EDOT}} = 2$) a strong dependence of the normalized MR with normalized M_{rev} is found, whereas for the polymer dominated case ($r_{\text{EDOT}} = 10$) there is practically no effect; $r_{\text{EDOT}} = 5$, as before, shows an intermediate behavior. In this way, Figure 12 reveals that the M_{rev} dependence of MR% can be scaled for the composites above a minimum concentration of MNP and confirms that

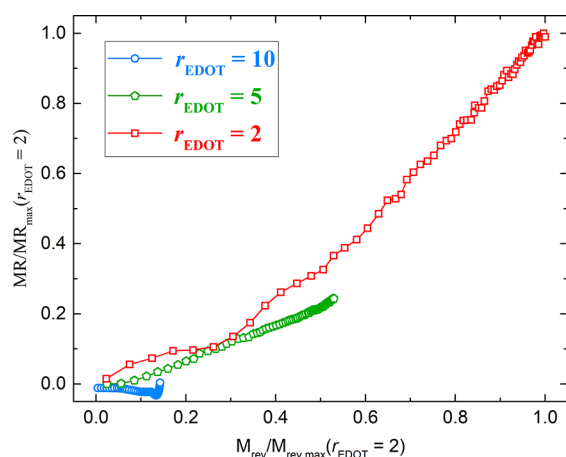


Figure 12. Normalized relative magnetoresistance vs relative reversible magnetization for CoFe_2O_4 -PEDOT composites with different r_{EDOT} molar ratios.

the magnitude of the observed magnetoresistance is a function of the reversible term of the magnetization.

These results give an interesting clue about the microscopic origin of MR for these composites. Indeed, the nonhysteretic behavior of MR ruled out that the magnetoresistance could be related to an interaction between the electrical carriers and the magnetic moments of MNP or their local magnetic field. Discarding its direct magnetic origin, but considering its dependence with M_{rev} , the magnetic-field-induced rotation of the MNP can be considered as its possible source. In this context, rotation of MNP could stretch the polymer chains as well as narrowing their local section, being consistently two contributions that produce a positive magnetoresistance. Further studies are needed to confirm this hypothesis.

CONCLUSIONS

Composites based on MNP of CoFe_2O_4 and the conducting polymer PEDOT in different molar ratios were synthesized chemically by using DBSA as acid media and nanoparticles protecting agent. In these materials the nanoparticles are aggregated in clusters, and the morphology depends on r_{EDOT} . It was also found that the electrical conductivity of the composites decreases as r_{EDOT} increases, being in the range 10^{-5} – 10^{-3} S cm^{-1} . These values indicate that the inclusion of MNP has a long-range effect in the electrical conductivity of PEDOT, which is probably related to the generation of mechanical stress and to a change in the electrical mobility of carriers. From the magnetization experiments it can be concluded that in PEDOT- CoFe_2O_4 composites exist a RKKY interaction that strongly couples ferromagnetically all the MNP that are at distances less than the estimated interval for d_{FM} (3–13 nm), causing them to act as a single magnetic cluster, giving as a result an increase in the magnetization of saturation and in the remanence ratio with r_{EDOT} . On the other hand, between magnetic clusters exist dipolar interactions, the magnitude of which decreases with the increase in r_{EDOT} . The composites also exhibit positive and reversible magnetoresistance, the magnitude of which increases with the applied magnetic field and decreases with increasing r_{EDOT} , being negligible for pure PEDOT. The applied magnetic field induces the rotation of the MNP, a phenomenon that could stretch the polymer chains as well narrowing their local section, giving as a result an increase in the magnetoresistance with the

applied magnetic field. Moreover, for the composite with $r_{\text{EDOT}} = 2$ the maximum MR% is 0.7%, and there is also a linear relationship between the MR% and H in the low field region. This last result favors considering this material as a promising candidate to be applied as a magnetic sensor. All the results obtained and the analysis performed in this work allows to have a physical understanding of the magnetic interactions and their relationship with r_{EDOT} —facts that are very important for the future application of these composite materials.

AUTHOR INFORMATION

Corresponding Author

P. Soledad Antonel — Instituto de Química Física de Materiales, Ambiente y Energía (INQUIMAE) and Departamento de Química Inorgánica, Analítica y Química Física, Facultad de Ciencias Exactas y Naturales, Universidad de Buenos Aires, C1428EGA Buenos Aires, Argentina; orcid.org/0000-0001-6454-6481; Email: sole@qi.fcen.uba.ar

Authors

Matías Lanús Mendez Elizalde — Instituto de Química Física de Materiales, Ambiente y Energía (INQUIMAE) and Departamento de Química Inorgánica, Analítica y Química Física, Facultad de Ciencias Exactas y Naturales, Universidad de Buenos Aires, C1428EGA Buenos Aires, Argentina

Carlos Acha — Laboratorio de Bajas Temperaturas, Departamento de Física, Facultad de Ciencias Exactas y Naturales, Universidad de Buenos Aires and IFIBA (UBA-CONICET), C1428EHA Buenos Aires, Argentina

Fernando V. Molina — Instituto de Química Física de Materiales, Ambiente y Energía (INQUIMAE) and Departamento de Química Inorgánica, Analítica y Química Física, Facultad de Ciencias Exactas y Naturales, Universidad de Buenos Aires, C1428EGA Buenos Aires, Argentina

Complete contact information is available at:

<https://pubs.acs.org/10.1021/acs.jpcc.9b11241>

Author Contributions

The manuscript was written through contributions of all authors. M.L.M.E. performed the experimental part; C.A. devised and supervised IRM, DCD, magnetoresistance, and conductivity measurements; M.L.M.E., C.A., and P.S.A. analyzed the results; F.V.M. contributed with the discussions; P.S.A. devised and supervised all the experiments and wrote the manuscript. All authors have given approval to the final version of the manuscript.

Notes

The authors declare no competing financial interest.

ACKNOWLEDGMENTS

The authors gratefully acknowledge funding from the Universidad de Buenos Aires (Grants 20020130100035BA, 20020170100284BA, and 20020120300007BA) and the Agencia Nacional de Promoción Científica y Tecnológica (Grants PICT 2014 no. 2289 and no. 1194), all of Argentina. The collaborations of A. G. Leyva in the thermogravimetric measurements and of G. Lavorato in HR-TEM measurements are gratefully acknowledged. P.S.A., C.A., and F.V.M. are members of the Carrera del Investigador Científico of CONICET.

REFERENCES

- (1) Deng, J.; He, C.; Peng, Y.; Wang, J.; Long, X.; Li, P.; Chan, A. S. C. Magnetic and Conductive Fe₃O₄-Polyaniline Nanoparticles with Core-Shell Structure. *Synth. Met.* **2003**, *139* (2), 295–301.
- (2) Reddy, K. R.; Park, W.; Sin, B. C.; Noh, J.; Lee, Y. Synthesis of Electrically Conductive and Superparamagnetic Monodispersed Iron Oxide-Conjugated Polymer Composite Nanoparticles by in Situ Chemical Oxidative Polymerization. *J. Colloid Interface Sci.* **2009**, *335* (1), 34–39.
- (3) Antonel, P. S.; Berhó, F. M.; Jorge, G.; Molina, F. V. Magnetic Composites of CoFe₂O₄ Nanoparticles in a Poly(Aniline) Matrix: Enhancement of Remanence Ratio and Coercivity. *Synth. Met.* **2015**, *199*, 292–302.
- (4) Yang, C.; Du, J.; Peng, Q.; Qiao, R.; Chen, W.; Xu, C.; Shuai, Z.; Gao, M. Polyaniline/Fe₃O₄ Nanoparticle Composite: Synthesis and Reaction Mechanism. *J. Phys. Chem. B* **2009**, *113* (15), 5052–5058.
- (5) Zhang, H.; Zhong, X.; Xu, J.-J.; Chen, H.-Y. Fe₃O₄/Polypyrrole/Au Nanocomposites with Core/Shell/Shell Structure: Synthesis, Characterization, and Their Electrochemical Properties. *Langmuir* **2008**, *24* (23), 13748–13752.
- (6) Xuan, S.; Wang, Y.-X. J.; Yu, J. C.; Leung, K. C.-F. Preparation, Characterization, and Catalytic Activity of Core/Shell Fe₃O₄@polyaniline@Au Nanocomposites. *Langmuir* **2009**, *25* (19), 11835–11843.
- (7) Guo, J.; Gu, H.; Wei, H.; Zhang, Q.; Haldolaarachchige, N.; Li, Y.; Young, D. P.; Wei, S.; Guo, Z. Magnetite-Polypyrrole Metacomposites: Dielectric Properties and Magnetoresistance Behavior. *J. Phys. Chem. C* **2013**, *117* (19), 10191–10202.
- (8) Li, Y.; Chen, G.; Li, Q.; Qiu, G.; Liu, X. Facile Synthesis, Magnetic and Microwave Absorption Properties of Fe₃O₄/Polypyrrole Core/Shell Nanocomposite. *J. Alloys Compd.* **2011**, *509* (10), 4104–4107.
- (9) Gandhi, N.; Singh, K.; Ohlan, A.; Singh, D. P.; Dhawan, S. K. Thermal, Dielectric and Microwave Absorption Properties of Polyaniline-CoFe₂O₄ Nanocomposites. *Compos. Sci. Technol.* **2011**, *71* (15), 1754–1760.
- (10) Ahmad, H.; Kumar, K.; Rahman, M. A.; Rahman, M. M.; Miah, M. A. J.; Minami, H.; Nuri, M. A. Preparation and Characterization of Conducting Polyaniline Layered Magnetic Nano Composite Polymer Particles. *Polym. Adv. Technol.* **2013**, *24* (8), 740–746.
- (11) Radhakrishnan, S.; Rao, C. R. K.; Vijayan, M. Performance of Conducting Polyaniline-DBSA and Polyaniline-DBSA/Fe₃O₄ Composites as Electrode Materials for Aqueous Redox Supercapacitors. *J. Appl. Polym. Sci.* **2011**, *122* (3), 1510–1518.
- (12) Chandrasekhar, P. *Conducting Polymers, Fundamentals and Applications*; Springer: Boston, MA, 1999.
- (13) Lizarraga, L.; Andrade, E. M.; Molina, F. V. Swelling and Volume Changes of Polyaniline upon Redox Switching. *J. Electroanal. Chem.* **2004**, *561*, 127–135.
- (14) Antonel, P. S.; Völker, E.; Molina, F. V. Photophysics of Polyaniline: Sequence-Length Distribution Dependence of Photoluminescence Quenching as Studied by Fluorescence Measurements and Monte Carlo Simulations. *Polymer* **2012**, *53* (13), 2619–2627.
- (15) De Oliveira, T. V. A. G.; Gobbi, M.; Porro, J. M.; Hueso, L. E.; Bittner, A. M. Charge and Spin Transport in PEDOT:PSS Nanoscale Lateral Devices. *Nanotechnology* **2013**, *24* (47), 475201.
- (16) Yamato, H.; Ohwa, M.; Wernet, W. Stability of Polypyrrole and Poly(3,4-Ethylenedioxythiophene) for Biosensor Application. *J. Electroanal. Chem.* **1995**, *397* (1–2), 163–170.
- (17) Aleshin, A. N.; Kiebooms, R.; Heeger, A. J. Metallic Conductivity of Highly Doped Poly(3,4-Ethylenedioxythiophene). *Synth. Met.* **1999**, *101* (1–3), 369–370.
- (18) Pei, Q.; Zuccarello, G.; Ahlskog, M.; Inganäs, O. Electrochromic and Highly Stable Poly(3,4-Ethylenedioxythiophene) Switches between Opaque Blue-Black and Transparent Sky Blue. *Polymer* **1994**, *35* (7), 1347–1351.
- (19) Kodama, R. H. Magnetic Nanoparticles. *J. Magn. Magn. Mater.* **1999**, *200* (1–3), 359–372.
- (20) Beveridge, J. S.; Stephens, J. R.; Williams, M. E. The Use of Magnetic Nanoparticles in Analytical Chemistry. *Annu. Rev. Anal. Chem.* **2011**, *4* (1), 251–273.
- (21) Mazarío, E.; Herrasti, P.; Morales, M. P.; Menéndez, N. Synthesis and Characterization of CoFe₂O₄ Ferrite Nanoparticles Obtained by an Electrochemical Method. *Nanotechnology* **2012**, *23* (35), 355708.
- (22) Kim, Y. Il; Kim, D.; Lee, C. S. Synthesis and Characterization of CoFe₂O₄Magnetic Nanoparticles Prepared by Temperature-Controlled Coprecipitation Method. *Phys. B* **2003**, *337* (1–4), 42–51.
- (23) Singh, K.; Ohlan, A.; Bakhshi, A. K.; Dhawan, S. K. Synthesis of Conducting Ferromagnetic Nanocomposite with Improved Microwave Absorption Properties. *Mater. Chem. Phys.* **2010**, *119* (1–2), 201–207.
- (24) Bhaumik, M.; Leswif, T. Y.; Maity, A.; Srinivasu, V. V.; Onyango, M. S. Removal of Fluoride from Aqueous Solution by Polypyrrole/Fe₃O₄Magnetic Nanocomposite. *J. Hazard. Mater.* **2011**, *186* (1), 150–159.
- (25) Shin, S.; Yoon, H.; Jang, J. Polymer-Encapsulated Iron Oxide Nanoparticles as Highly Efficient Fenton Catalysts. *Catal. Commun.* **2008**, *10* (2), 178–182.
- (26) Sen, P.; De, A. Electrochemical Performances of Poly(3,4-Ethylenedioxythiophene)-NiFe₂O₄ Nanocomposite as Electrode for Supercapacitor. *Electrochim. Acta* **2010**, *55* (16), 4677–4684.
- (27) Lu, Z.; Yu, Z.; Dong, J.; Xiong, X.; Gao, L.; Song, M.; Liu, Y.; Fan, D.; Yan, Y.; Huo, P. Enhanced Photocatalytic Activity and Selectivity of a Novel Magnetic PW@PEDOT Imprinted Photocatalyst with Good Reproducibility. *Nano* **2018**, *13* (2), 1850020.
- (28) Ohlan, A.; Singh, K.; Chandra, A.; Dhawan, S. K. Microwave Absorption Behavior of Core-Shell Structured Poly(3,4-Ethylenedioxy Thiophene)-Barium Ferrite Nanocomposites. *ACS Appl. Mater. Interfaces* **2010**, *2* (3), 927–933.
- (29) Shin, S.; Jang, J. Thiol Containing Polymer Encapsulated Magnetic Nanoparticles as Reusable and Efficiently Separable Adsorbent for Heavy Metal Ions. *Chem. Commun.* **2007**, No. 41, 4230–4232.
- (30) Abou-Elazab, T. F.; Migahed, M. D.; Park, H.; Park, Y. W.; MacNeillis, P.; Rabenau, T.; Roth, S. Magnetoresistance of Polypyrrole and Polyacetylene. *Synth. Met.* **1996**, *76* (1–3), 281–284.
- (31) Klemm, P.; Bange, S.; Pöllmann, A.; Boehme, C.; Lupton, J. M. Nanoscale Magnetoresistance in π -Conjugated Polymer Devices. *Phys. Rev. B: Condens. Matter Mater. Phys.* **2017**, *95* (24), 241407.
- (32) Long, Y.; Chen, Z.; Shen, J.; Zhang, Z.; Zhang, L.; Huang, K.; Wan, M.; Jin, A.; Gu, C.; Duvail, J. L. Magnetoresistance Studies of Polymer Nanotube/Wire Pellets and Single Polymer Nanotubes/Wires. *Nanotechnology* **2006**, *17* (24), 5903–5911.
- (33) Chutia, P.; Kumar, A. Temperature- and Magnetic Field-Dependent Electrical Transport Studies of Poly(3,4-Ethylenedioxythiophene) Nanoparticles. *J. Nanopart. Res.* **2014**, DOI: 10.1007/s11051-014-2617-6.
- (34) Gobbi, M.; Orgiu, E. The Rise of Organic Magnetoresistance: Materials and Challenges. *J. Mater. Chem. C* **2017**, *5* (23), 5572–5580.
- (35) Venkatesan, M.; Nawka, S.; Pillai, S. C.; Coey, J. M. D. Enhanced Magnetoresistance in Nanocrystalline Magnetite. *J. Appl. Phys.* **2003**, *93* (10), 8023–8025.
- (36) Bham, S. D.; Joy, P. A. Tuning of the Magnetostrictive Properties of CoFe₂O₄ by Mn Substitution for Co. *J. Appl. Phys.* **2006**, *100* (11), 113911.
- (37) Msomi, J. Z.; Moyo, T.; Abdallah, H. M. I.; Dolo, J. J. Electrical and Magnetoresistance Properties of Mg_xMn_{1-x}Fe₂O₄ Compounds. *J. Supercond. Novel Magn.* **2013**, *26* (4), 1021–1025.
- (38) Majumdar, S.; Grochowska, K.; Sawczak, M.; Liwiński, G.; Huhtinen, H.; Dahl, J.; Tuominen, M.; Laukkanen, P.; Majumdar, H. S. Interfacial Properties of Organic Semiconductor-Inorganic Magnetic Oxide Hybrid Spintronic Systems Fabricated Using Pulsed Laser Deposition. *ACS Appl. Mater. Interfaces* **2015**, *7* (40), 22228–22237.

- (39) Gu, H.; Zhang, X.; Wei, H.; Huang, Y.; Wei, S.; Guo, Z. An Overview of the Magnetoresistance Phenomenon in Molecular Systems. *Chem. Soc. Rev.* **2013**, *42* (13), 5907–5943.
- (40) Guo, L.; Gu, X.; Zhu, X.; Sun, X. Recent Advances in Molecular Spintronics: Multifunctional Spintronic Devices. *Adv. Mater.* **2019**, *31* (45), 1805355.
- (41) Romero, M.; Faccio, R.; Pardo, H.; Tumelero, M. A.; Montenegro, B.; Campos Plá Cid, C.; Pasa, A. A.; Momburá, Á. W. The Effect of Manganite Nanoparticle Addition on the Low Field Magnetoresistance of Polyaniline. *J. Mater. Chem. C* **2015**, *3* (46), 12040–12047.
- (42) Gu, H.; Huang, Y.; Zhang, X.; Wang, Q.; Zhu, J.; Shao, L.; Haldolaarachchige, N.; Young, D. P.; Wei, S.; Guo, Z. Magnetoresistive Polyaniline-Magnetite Nanocomposites with Negative Dielectrical Properties. *Polymer* **2012**, *53* (3), 801–809.
- (43) Paterno, L. G.; Soler, M. A. G.; Fonseca, F. J.; Sinnecker, J. P.; Sinnecker, E. H. C. P.; Lima, E. C. D.; Novak, M. A.; Morais, P. C. Layer-by-Layer Assembly of Bifunctional Nanofilms: Surface-Functionalized Maghemite Hosted in Polyaniline. *J. Phys. Chem. C* **2009**, *113* (13), 5087–5095.
- (44) Soler, M. A. G.; Paterno, L. G.; Sinnecker, J. P.; Wen, J. G.; Sinnecker, E. H. C. P.; Neumann, R. F.; Bahiana, M.; Novak, M. A.; Morais, P. C. Assembly of γ -Fe₂O₃/Polyaniline Nanofilms with Tuned Dipolar Interaction. *J. Nanopart. Res.* **2012**, DOI: 10.1007/s11051-011-0653-z.
- (45) Muñoz Resta, I.; Sellés, J. M.; Lanús Méndez Elizalde, M.; Antonel, P. S.; Molina, F. V. Polypyrrole-CoFe₂O₄ Nanocomposites: Polymer Influence on Magnetic Behavior and Particle Effects on Polymer Conduction. *Polym. Compos.* **2018**, *39* (12), 4617–4627.
- (46) Zhou, W.; Hu, X.; Bai, X.; Zhou, S.; Sun, C.; Yan, J.; Chen, P. Synthesis and Electromagnetic, Microwave Absorbing Properties of Core-Shell Fe₃O₄-Poly(3,4-Ethylenedioxythiophene) Microspheres. *ACS Appl. Mater. Interfaces* **2011**, *3* (10), 3839–3845.
- (47) Antonel, P. S.; Jorge, G.; Perez, O. E.; Butera, A.; Leyva, A. G.; Negri, R. M. Magnetic and Elastic Properties of CoFe₂O₄ - Polydimethylsiloxane Magnetically Oriented Elastomer Nanocomposites. *J. Appl. Phys.* **2011**, *110* (4), 043920.
- (48) Ohlan, A.; Singh, K.; Chandra, A.; Dhawan, S. K. Microwave Absorption Behavior of Core - Shell Structured Poly (3,4 - Ethylenedioxy Thiophene) - Barium Ferrite Nanocomposites. *ACS Appl. Mater. Interfaces* **2010**, *2* (3), 927–933.
- (49) Schulman, A.; Lanosa, L. F.; Acha, C. Poole-Frenkel Effect and Variable-Range Hopping Conduction in Metal/YBCO Resistive Switching Devices. *J. Appl. Phys.* **2015**, *118* (4), 2–8.
- (50) Klemm, P.; Bange, S.; Pöllmann, A.; Boehme, C.; Lupton, J. M. Nanoscale Magnetoresistance in π -Conjugated Polymer Devices. *Phys. Rev. B: Condens. Matter Mater. Phys.* **2017**, *95* (24), 1–6.
- (51) Qu, Y.; Yang, H.; Yang, N.; Fan, Y.; Zhu, H.; Zou, G. The Effect of Reaction Temperature on the Particle Size, Structure and Magnetic Properties of Coprecipitated CoFe₂O₄ Nanoparticles. *Mater. Lett.* **2006**, *60* (29–30), 3548–3552.
- (52) Hu, J.-M.; Sheng, G.; Zhang, J. X.; Nan, C. W.; Chen, L. Q. Phase-Field Simulation of Strain-Induced Domain Switching in Magnetic Thin Films. *Appl. Phys. Lett.* **2011**, *98* (11), 112505.
- (53) Gajbhiye, N.S.; Prasad, S.; Blaji, G. Experimental Study of Hopkinson Effect in Single Domain CoFe₂O₄ Particles. *IEEE Trans. Magn.* **1999**, *35* (4), 2155–2161.
- (54) Sun, S.; Zeng, H.; Robinson, D. B.; Raoux, S.; Rice, P. M.; Wang, S. X.; Li, G. Monodisperse MFe₂O₄ (M = Fe, Co, Mn) Nanoparticles. *J. Am. Chem. Soc.* **2004**, *126* (1), 273–279.
- (55) Kambale, R. C.; Shaikh, P. A.; Harale, N. S.; Bilur, V. A.; Kolekar, Y. D.; Bhosale, C. H.; Rajpure, K. Y. Structural and Magnetic Properties of Co_{1-x}MnxFe₂O₄ (0 ≤ x ≤ 0.4) Spinel Ferrites Synthesized by Combustion Route. *J. Alloys Compd.* **2010**, *490* (1–2), 568–571.
- (56) Awad, K. R.; Wahsh, M. M. S.; Othman, A. G. M.; Girgis, E.; Mabrouk, M. R.; Morsy, F. A. Effect of Mn²⁺ Doping and SiO₂ Coating on Magneto-Optical Properties of CoFe₂O₄ Nano-Particles. *Smart Mater. Struct.* **2015**, *24* (11), 115002.
- (57) Kurian, M.; Thankachan, S.; Nair, D. S.; E. K., A.; Babu, A.; Thomas, A.; Krishna K. T., B. Structural, Magnetic, and Acidic Properties of Cobalt Ferrite Nanoparticles Synthesised by Wet Chemical Methods. *J. Adv. Ceram.* **2015**, *4* (3), 199–205.
- (58) Choi, J. W.; Han, M. G.; Kim, S. Y.; Oh, S. G.; Im, S. S. Poly(3,4-Ethylenedioxythiophene) Nanoparticles Prepared in Aqueous DBSA Solutions. *Synth. Met.* **2004**, *141* (3), 293–299.
- (59) Morvant, M. C.; Reynolds, J. R. In Situ Conductivity Studies of Poly(3,4-Ethylenedioxythiophene). *Synth. Met.* **1998**, *92* (1), 57–61.
- (60) Corradi, R.; Armes, S. P. Chemical Synthesis of Poly(3,4-Ethylenedioxythiophene). *Synth. Met.* **1997**, *84* (1–3), 453–454.
- (61) McLachlan, D. S. An Equation for the Conductivity of Binary Mixtures with Anisotropic Grain Structures. *J. Phys. C: Solid State Phys.* **1987**, *20* (7), 865–877.
- (62) McLachlan, D. S.; Blaszkiewicz, M.; Newnham, R. E. Electrical Resistivity of Composites. *J. Am. Ceram. Soc.* **1990**, *73* (8), 2187–2203.
- (63) Kumar, S. S.; Kumar, C. S.; Mathiyarasu, J.; Phani, K. L. Stabilized Gold Nanoparticles by Reduction Using 3,4-Ethylenedioxythiophene-Polystyrenesulfonate in Aqueous Solutions: Nanocomposite Formation, Stability, and Application in Catalysis. *Langmuir* **2007**, *23* (6), 3401–3408.
- (64) Selvaganesh, S. V.; Mathiyarasu, J.; Phani, K. L. N.; Yegnanaram, V. Chemical Synthesis of PEDOT-Au Nanocomposite. *Nanoscale Res. Lett.* **2007**, *2* (11), 546–549.
- (65) Chinnasamy, C.N.; Jeyadevan, B.; Perales-Perez, O.; Shinoda, K.; Tohji, K.; Kasuya, A. Growth Dominant Co-Precipitation Process to Achieve High Coercivity at Room Temperature in CoFe₂O₄ Nanoparticles. *IEEE Trans. Magn.* **2002**, *38* (5), 2640–2642.
- (66) Leslie-Pelecky, D. L.; Rieke, R. D. Magnetic Properties of Nanostructured Materials. *Chem. Mater.* **1996**, *8* (8), 1770–1783.
- (67) Safi, R.; Ghasemi, A.; Shoja-Razavi, R.; Tavousi, M. The Role of PH on the Particle Size and Magnetic Consequence of Cobalt Ferrite. *J. Magn. Magn. Mater.* **2015**, *396*, 288–294.
- (68) Zhang, H.; Zeng, D.; Liu, Z. The Law of Approach to Saturation in Ferromagnets Originating from the Magnetocrystalline Anisotropy. *J. Magn. Magn. Mater.* **2010**, *322* (16), 2375–2380.
- (69) Muñoz Resta, I.; Horwitz, G.; Lanús Méndez Elizalde, M.; Jorge, G. A.; Molina, F. V.; Antonel, P. S. Magnetic and Conducting Properties of Composites of Conducting Polymers and Ferrite Nanoparticles. *IEEE Trans. Magn.* **2013**, *49* (8), 4598–4601.
- (70) Kittel, C. *Quantum Theory of Solids*, 2nd revised ed.; John Wiley & Sons, Ltd.: Hoboken, NJ, 1987; Chapter 18.
- (71) Shi, W.; Zhao, T.; Xi, J.; Wang, D.; Shuai, Z. Unravelling Doping Effects on PEDOT at the Molecular Level: From Geometry to Thermoelectric Transport Properties. *J. Am. Chem. Soc.* **2015**, *137* (40), 12929–12938.
- (72) Wei, Q.; Mukaida, M.; Ishida, T. Extracting Carrier Mobility in Conducting Polymers Using a Photoinduced Charge Transfer Reaction. *J. Phys. Chem. C* **2018**, *122* (28), 15922–15928.
- (73) Gueye, M. N.; Carella, A.; Faure-Vincent, J.; Demadrille, R.; Simonato, J. P. Progress in Understanding Structure and Transport Properties of PEDOT-Based Materials: A Critical Review. *Prog. Mater. Sci.* **2020**, *108*, 100616.
- (74) El-Sayed, H. M. Evidence on the Presence of Ruderman–Kittel–Kasuya–Yosida (RKKY) Interaction in CoFe₂O₄@Au Nano Structure. *Superlattices Microstruct.* **2016**, *91*, 98–104.
- (75) García-Otero, J.; Porto, M.; Rivas, J. Henkel Plots of Single-Domain Ferromagnetic Particles. *J. Appl. Phys.* **2000**, *87* (10), 7376–7381.
- (76) Wohlfarth, E. P. Relations between Different Modes of Acquisition of the Remanent Magnetization of Ferromagnetic Particles. *J. Appl. Phys.* **1958**, *29* (3), 595–596.
- (77) Che, X.; Neal Bertram, H. Phenomenology of ΔM Curves and Magnetic Interactions. *J. Magn. Magn. Mater.* **1992**, *116* (1–2), 121–127.